Jpn. J. Cancer Res. **92**, 109–118, February 2001

Hexosaminidase-altered Aberrant Crypts, Carrying Decreased Hexosaminidase α and β Subunit mRNAs, in Colon of 1,2-Dimethylhydrazine-treated Rats

Tetsuya Tsukamoto,[1,4] Hiroko Fukami,[1] Shoji Yamanaka,[2] Akira Yamaguchi,[2] Hayao Nakanishi,[1] Hiroki Sakai,[1,3] Ichiro Aoki[2] and Masae Tatematsu[1]

[1]Division of Oncological Pathology, Aichi Cancer Center Research Institute, 1-1 Kanokoden, Chikusa-ku, Nagoya 464-8681, [2]Department of Pathology, Yokohama City University, School of Medicine, 3-9 Fukuura, Kanazawa-ku, Yokohama 236-8567 and [3]Department of Veterinary Pathology, Gifu University, 1-1 Yanagido, Gifu 501-1193

Aberrant crypt foci (ACF), consisting of morphologically irregular crypts, are thought to be precancerous lesions for colon cancers. For their molecular analysis, it is necessary to avoid contamination with adjacent normal crypts and stromal cells. Decreased hexosaminidase activity in ACF, which has been histochemically demonstrated, was used in the present study to classify isolated crypts in combination with morphological changes. The length, rim diameter, and width (average±SD, μm) of hexosaminidase-positive (Hex+) crypts were 238.6±40.4, 89.5±22.9, and 57.6±14.0, respectively. For hexosaminidase-negative (Hex−) crypts, the values were 314.4±77.8, 140.3±45.7, and 97.3±34.7, the width being 1.69 times greater ($P<0.0001$). Crypts wider than 115 μm (approximately 2 times the average size of Hex+ crypts) were all from ACF, judging from hexosaminidase staining. To analyze transcription levels of Hex α and β subunits (*Hexa* and *Hexb*, respectively), real-time relative quantitative reverse transcription-polymerase chain reaction (RT-PCR) analysis was performed using the LightCycler system. In aberrant crypts, both *Hexa* and *Hexb* were significantly down-regulated to 0.266 ($P<0.002$) and 0.131 ($P<0.001$) units, respectively, compared with those in morphologically normal crypts, with *β-actin* as the internal standard. This decrease could be a molecular marker for precancerous enzyme-altered ACF.

Key words: Aberrant crypt foci — Enzyme (hexosaminidase)-altered foci — Crypt isolation — Real-time PCR — LightCycler

The histogenesis of colon tumors involves a series of micro- and macroscopic mucosal lesions, ranging from aberrant crypt foci (ACF) to benign tumors and malignant cancers. By means of microscopic examination of methylene blue-stained mucosa, ACF as small as single crypts can be detected.[1)] The characterization of such early precursor lesions of colon cancer should increase our understanding of oncogenesis, these having been proposed as putative preneoplastic lesions by Bird in 1987.[2)] They are induced by administration of colon carcinogens in a dose-dependent manner,[3)] and histopathological assessment has shown that they may be either indistinguishable from normal, or adenomatous with marked cellular atypia in rats,[4)] but they generally have an elevated proliferation index.[5)]

In addition to morphological change, functional or biochemical alterations may occur in preneoplastic lesions. In colon, alteration of hexosaminidase activity has been reported to be linked with neoplasms in humans[6, 7)] and rodents.[8)] Enzyme-altered foci (EAF) have been proposed by Pretlow and colleagues[9, 10)] as one of the earliest colonic crypt lesions. They analyzed EAF in unembedded or whole-mount preparations of colons from carcinogen-treated rats, and found two populations of enzyme-altered crypts including examples which were morphologically aberrant and others which appeared normal.[11)] EAF, along with ACF, have been used as biomarkers for assessment of the effect of genotoxic[12–14)] and nongenotoxic[14)] carcinogens as well as chemopreventive agents.[15)]

β-Hexosaminidase/*N*-acetyl-β-D-glucosaminidase (EC 3.2.1.52) is a lysosomal enzyme. The *HEXA* and *HEXB* genes encode the β-hexosaminidase α- and β-subunits, respectively, which dimerize to produce two major forms of the enzyme, A (acidic, αβ dimer) and B (basic, ββ dimer) and a minor form, S (αα dimer), among which the A isozyme degrades G_{M2} gangliosides in concert with the G_{M2} activator, a ganglioside binding protein encoded by the *GM2A* gene. In man, mutations in the *HEXA* and *HEXB* genes are known to cause Tay-Sachs and Sandhoff diseases, respectively.[16)] The mouse *Hexa* and the *Hexb* genes have been cloned[17)] and knockout mice[18, 19)] have been developed as human G_{M2} gangliosidosis models, but they have not so far been studied in relation to the development of ACF and colon carcinogenesis.

To clarify whether ACF are directly related to carcinogenesis or are just innocent bystanders incidental to carcinogen exposure, it is necessary to analyze crypts individually. However, ACF have been simply defined as having an aberrant appearance when viewed on the mucosal surface. Thus, to establish criteria for selection of aber-

[4] To whom correspondence should be addressed.
E-mail: ttsukamt@aichi-cc.pref.aichi.jp

rant crypts upon crypt isolation,[20–22] hexosaminidase staining was utilized to distinguish aberrant crypts from normal ones. For comparison of selected isolated aberrant crypts with 'normal' counterparts, molecular analysis of the expression of hexosaminidase α- and β- subunit mRNAs was performed with *β-actin* mRNA as a reference, with the real-time relative quantitative reverse transcription-polymerase chain reaction (RT-PCR) utilizing a LightCycler system to measure the decreased mRNA levels.

MATERIALS AND METHODS

Animals Five-week-old male Fischer rats were purchased from Charles River Japan Inc. (Kanagawa) and maintained on basal diet (Oriental NMF, Oriental Yeast Co., Tokyo) and water *ad libitum* and housed in plastic cages in an air-conditioned room at 24°C with a 12 h light-12 h dark cycle.

Experimental protocol 1,2-Dimethylhydrazine·2HCl (Tokyo Chemical Industry, Tokyo) was injected subcutaneously at 20 mg/kg body weight once a week for 10 weeks. Animals were euthanized at experimental weeks 10 and 20.

Crypt isolation The distal half of the colonic epithelium was isolated and treated with 30 m*M* ethylenediaminetetraacetic acid (EDTA) (Dojin, Kumamoto) in Hanks' balanced salt solution. The crypts were isolated as described elsewhere,[20–22] and fixed either in 2% paraformaldehyde in 0.1 *M* phosphate buffer, pH 7.2 for 2 h for hexosaminidase staining or in 70% ethanol for molecular analysis.

Hexosaminidase staining The procedure for hexosaminidase staining was as described by Hayashi[23] with slight modifications.[24] Briefly, the working solution was prepared as follows: 3 mg of naphthol AS-BI *N*-acetyl-β-glucosaminide (Sigma, St. Louis, MO) was dissolved in 5 ml of ethylene glycol monomethyl ether (Nacalai Tesque, Kyoto), and 9.5 ml of 0.1 *M* citrate buffer, pH 4.7 and 10 mg of fast garnet GBC (Sigma) was added. Paraformaldehyde-fixed isolated crypts were washed in phosphate-buffered saline, pH 7.4, three times and incubated in the working solution for 30 min at 37°C.

Comparison of dimensions of hexosaminidase-positive (Hex+) and negative (Hex−) crypts The length, rim diameter and width of 121 Hex+ and 134 Hex− crypts were measured using a micrometer under a microscope (Olympus, Tokyo) and values were compared statistically with the *t* test.[25] Distributions of the widths of Hex+ and Hex− crypts were standardized, and probabilities were calculated.[25]

Total RNA isolation from isolated crypts Ethanol-fixed isolated crypts were subjected to total RNA isolation as basically described[26–28] with slight modifications. Lysis solution (Solution D+) containing 4 *M* guanidine thiocyanate (Wako, Osaka), 25 m*M* sodium citrate (Wako), pH 7, 0.5% *N*-lauroylsarcosine sodium salt (Nakalai Tesque), 0.1 *M* 2-mercaptoethanol (Sigma) and 200 μg/ml proteinase K (Wako) was used instead of the original Solution D. Proteinase K was indispensable to lyse ethanol-fixed crypts. Single crypts were transferred to 0.5 ml microfuge tubes under a stereoscopic microscope. After 50 μl of Solution D+ was added, samples were vortexed for 15 s at maximum speed at room temperature, incubated for 10 min at 37°C, and again vortexed for 15 s at maximum speed. Lysis of the crypts was monitored under a stereoscopic microscope (Olympus). Then, 5 μl of 2 *M* sodium acetate, pH 4 (Wako), 50 μl of buffer-saturated phenol (Gibco BRL, Grand Island, NY), and 10 μl of chloroform-isoamyl alcohol mixture (24:1) (Wako) were added and mixed vigorously. Samples were cooled on ice and centrifuged for 15 min at 12 000 rpm. The top aqueous phase was transferred to a new 0.5 ml tube, mixed with 50 μl of isopropanol containing 1 μl of Ethachinmate (Nippon Gene, Toyama) to improve recovery, and incubated for 1 h at −20°C. Samples were precipitated by centrifugation for 15 min at 13 000 rpm, washed in 200 μl of pre-chilled 75% ethanol, air-dried, and redissolved in 9 μl of distilled water (Wako) at 50°C for 10 min.

Reverse transcription First-strand cDNA was synthesized as described[29] using the Thermoscript RT-PCR System (Gibco BRL) according to the manufacturer's instructions. Briefly, 1 μl of oligo$(dT)_{20}$ was added to 9 μl of RNA extracted above, and the mixture was incubated at 65°C for 5 min, and placed on ice. Then reverse transcription was performed in the presence of 5 m*M* dithiothreitol (DTT), 2 U/μl RNase inhibitor (RNaseOUT), 1 m*M* dNTP, and 0.375 units/μl Thermoscript Reverse Transcriptase at 50°C for 60 min. Reactions were terminated by heating at 85°C for 5 min and the products were stored at −20°C until use.

Relative quantitation of hexosaminidase α (*Hexa*) and β (*Hexb*) subunit mRNAs Relative quantitative PCR was performed with a LightCycler (Roche Diagnostics, Mannheim, Germany), with *β-actin* as the reference. PCR was performed basically as described[30] using a SYBR Green PCR Core Reagents kit (Perkin-Elmer Applied Biosystems, Foster City, CA). For the PCR, a 20 μl reaction mixture was used containing 2 μl of cDNA, 200 n*M* each of 5′ and 3′ primers, 200 μ*M* each of dATP, dCTP, and dGTP, 400 μ*M* dUTP, 1.5 (for *β-actin* and *Hexa*) or 3 (for *Hexb*) m*M* $MgCl_2$, 0.25 mg/ml deionized bovine albumin, fraction V (Sigma, Cat. No. A6918), 0.025 units/μl AmpliTaq Gold DNA polymerase and the provided buffer. The 5′- and 3′-primer sequences for amplification of rat *β-actin* gene were derived from exons 5 and 6, respectively.[31] Rat *Hexa* and *Hexb* cDNA were partially cloned (Yamaguchi *et al.*, manuscript in preparation) and primers, showing low similarity with each other, were selected in different exons (Table I). Mouse cDNA sequences[17] were used for

Table I. PCR Primer Sequences Used in the LightCycler Analysis

Description	Target	Sequences	Location	Product length (bp)
rBA3	*β-actin*	5′-GAC CTC TAT GCC AAC ACA GTG-3′ (sense)	exon 5	226
rBA4		5′-GGC CGG ACT CAT CGT A-3′ (antisense)	exon 6	
rhexa1	*Hexa*[a)]	5′-GGA AGA GAT GCC GGT CCA G-3′ (sense)	exon 11	177
rhexa2		5′-ACC AGA GCC TTT TGT GCA GGT-3′ (antisense)	exon 12	
rhexb1	*Hexb*[b)]	5′-AAA GAT TTT GGA TAT TAT CAC ATC C-3′ (sense)	exons 9–10	276
rhexb2		5′-ACA AGT TGT TTC TGC TTC TCC-3′ (antisense)	exon 12	

a) and *b*) Hexosaminidase α- and β- subunits.

deduction of primer localization. The PCR program was 95°C for 10 min to activate AmpliTaq Gold, followed by 50 cycles of 95°C for 60 s to denature, 60°C for 60 s for annealing, 72°C for 60 s for extension with a 20°C/s slope. SYBR Green fluorescence was measured at the end of each extension. Four to 5 normal and aberrant crypts each per animal were used to analyze *Hexa* and *Hexb* expression levels, normalized to the *β-actin* level for one set of experiments. Seven sets were performed.

RESULTS

Development of ACF Methylene blue staining of colon epithelium allowed ACF to be recognized (data not shown). Hexosaminidase staining showed ACF to be negatively dyed, surrounded by normal small round crypts having red grains (Fig. 1).

Hexosaminidase staining of isolated crypts Isolated crypts were detected with hexosaminidase staining as Hex+ and Hex− crypts as shown in Fig. 2A. Hex− crypts (Fig. 2B, arrow and arrowhead) had a wider crypt diameter than adjacent Hex+ crypts. They also appeared longer, with a greater rim diameter. The sizes of the isolated crypts were consistent with those of crypts in whole mounts (Fig. 1).

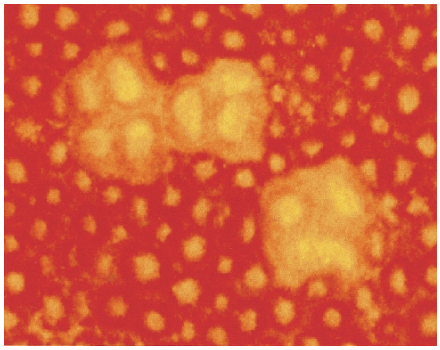

Fig. 1. ACF consisting of enlarged crypts are shown to be negative for hexosaminidase. Surrounding normal small round crypts are strongly stained.

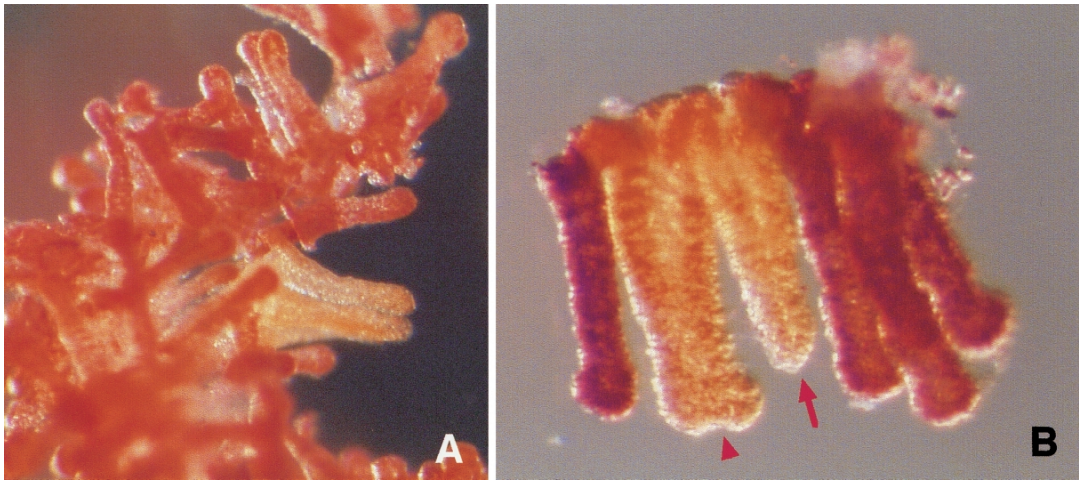

Fig. 2. (A) Hexosaminidase staining of roughly isolated crypts from colon of a 1,2-dimethylhydrazine (DMH)-treated rat, photographed under a stereoscopic microscope. (B) Hex− crypts (arrow and arrowhead) are longer and wider in crypt diameter and have a greater rim diameter than adjacent Hex+ crypts.

Size distribution of Hex+ and Hex− crypts One hundred and twenty-one Hex+ and 134 Hex− crypts were measured for length, rim diameter and width as illustrated in Fig. 3A. Histograms along with normal probability density functions were plotted (Fig. 3B). The average values (μ)±SD (σ) for these dimensions of Hex+ crypts were 238.6±40.4 μm, 89.5±22.9 μm, and 57.6±14.0 μm, respectively. For Hex− crypts, the values were 314.4±

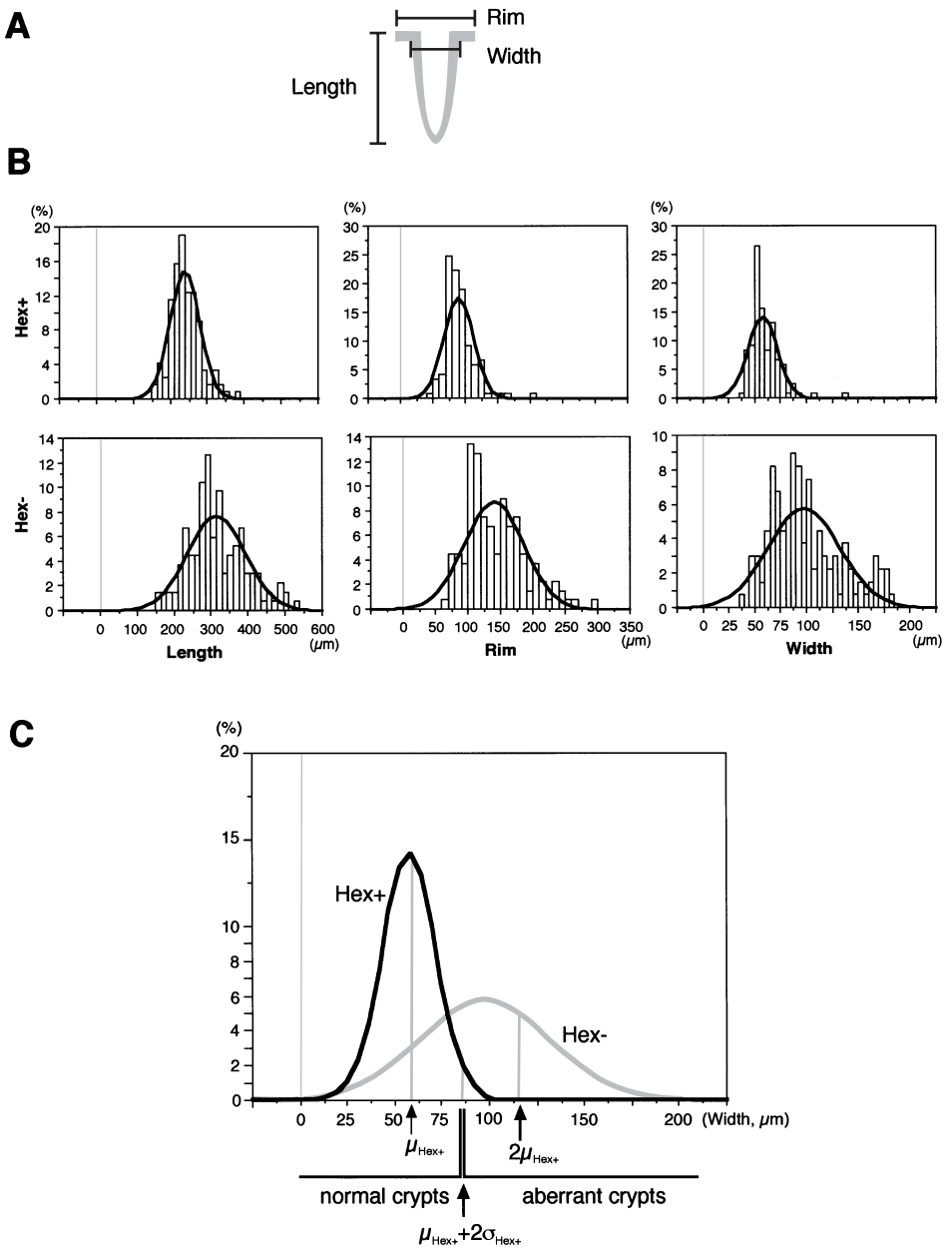

Fig. 3. (A) A scheme of a crypt showing which parts were measured for length, width, and rim diameter. (B) Histograms along with normal probability density functions. Average (μ)±SD (σ) (μm) values for Hex+ crypts' length, rim diameter, and width were 238.6±40.4, 89.5±22.9, and 57.6±4.0, respectively, and those for Hex− crypts were 314.4±77.8, 140.3±45.7, and 97.3±34.7. The length of Hex− crypts was 1.32 times longer, the rim diameter was 1.57 times bigger, and the width was 1.69 times wider, with statistical significance (P<0.0001). (C) Normal density functions of Hex+ and Hex− for width are superimposed. Crypts smaller than $\mu_{Hex+}+2\sigma_{Hex+}$ (85.6 μm) were judged as normal independent of staining, and those larger than this cut-off as aberrant crypts. With crypts bigger than $2\mu_{Hex+}$ (115.1 μm), where $\mu_{Hex-}+0.51\sigma_{Hex-}$ and $\mu_{Hex+}+4.1\sigma_{Hex+}$, the probabilities of being Hex− and Hex+ crypts were 0.304 and 2×10^{-5}, respectively.

77.8 μm, 140.3±45.7 μm, and 97.3±34.7 μm. Comparing the average sizes, the length of Hex− crypts was 1.32 times longer, the rim diameter was 1.57 times bigger, and the width was 1.69 times wider, all three increases being significant (P<0.0001). Since the difference of the width was the largest, it was chosen for further analysis.

As shown in Fig. 3C, the histogram of the width could be approximated as a normal distribution. With the average±2SD generally considered as the normal range, crypts smaller than $\mu+2\sigma$ for Hex+ crypts ($\mu_{Hex+}+2\sigma_{Hex+}$=85.6 μm) would be judged as normal and those larger than this as aberrant. When crypts larger than 2 μ_{Hex+} (115.1 μm) were considered, with $\mu_{Hex-}+0.51\sigma_{Hex-}$ for Hex− and $\mu_{Hex+}+4.1\sigma_{Hex+}$ for Hex+ distribution, the probabilities of being Hex− and Hex+ were 0.304 and 2×10^{-5}, respectively. Thus, it was possible to predict Hex− aberrant crypts only from size data with almost 100% probability.

Relative quantitative analysis of *Hexa* and *Hexb* subunit mRNAs Some crypts were fixed in 70% ethanol and stored at −20°C to preserve nucleic acids. Since these could not be visualized with Hex staining because of inactivation of the enzyme by the ethanol, crypts sized approximately 2 times normal crypts ($2\mu_{Hex+}$) were isolated for molecular analysis of expression levels of *β-actin*, *Hexa*, and *Hexb* using the LightCycler. Representative results are shown in Fig. 4A. The noise band cursor was set at a 1.18 fluorescence level to remove background, and the crossing line was adjusted to 9.86 in the linear exponential phase. The crossing points for *β-actin*, *Hexa*, and *Hexb* of an aberrant crypt were 25.35 (A_o), 31.02 (A_a), and 34.61 (A_b), and those for a normal fcrypt were 29.19 (N_o), 31.43 (N_a),

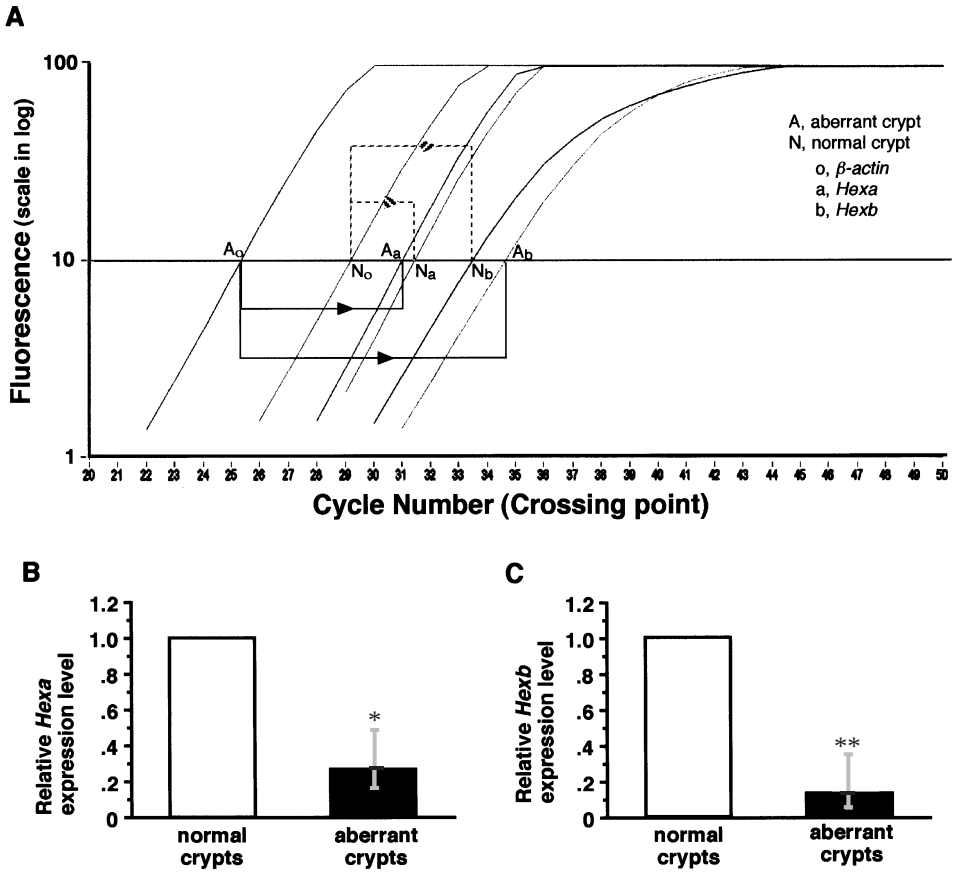

Fig. 4. (A) An example of the real-time relative quantitative RT-PCR analysis using the LightCycler system. The crossing points for *β-actin*, *Hexa*, and *Hexb* with an aberrant crypt were 25.35 (A_o), 31.02 (A_a), and 34.61 (A_b), and for a normal crypt, 29.19 (N_o), 31.43 (N_a), and 33.41 cycles (N_b). See "Results" for the detailed calculation. (B) Mean−SD, mean, and mean+SD for the ratio (R_{Aa}) of normalized *Hexa* expression in an aberrant crypt compared with a normal crypt were 0.152, 0.266, and 0.488, all values being significantly different from those for normal-looking crypts (∗ P<0.002), with R_{Na} set to be 1. (C) Similarly, for *Hexb* (R_{Ab}), mean−SD, mean, and mean+SD were 0.047, 0.130, and 0.360 with statistically significant differences from normal-looking crypts (∗∗ P<0.001), where R_{Nb} is set to be 1.

Table II. Relative Cycle Numbers of Normalized *Hexa* and *Hexb* of Aberrant Crypts Compared to Normal Crypts in the LightCycler Experiments[a)]

Experiment nos.	1	2	3	4	5	6	7	Ave±SD
Hexa	ND[d)]	−2.07	−1.83	−0.63	−3.12	−2.12	−1.69	−1.91±0.80[b)]
Hexb	−5.90	−2.48	−3.03	−2.03	−1.37	−2.33	−3.43	−2.94±1.47[c)]

a) Crossing points for *Hexa* and *Hexb* for each sample as shown in Fig. 4 were normalized with that for β-actin. Relative cycle numbers in aberrant crypts were calculated by subtraction of the value for normal crypts from that of aberrant crypts ($\log R_{Aa}$ and $\log R_{Ab}$, see "Results" for the calculation). Each value is an average from 4 or 5 crypts in each experiment. Overall averages of 6 or 7 experiments are described in the right-most column.
b) and *c*) Value for aberrant crypts is statistically significantly lower than that for normal crypts, which is 0, with the Mann-Whitney *U* test ($P<0.002$ and $P<0.001$, respectively).
d) ND, not done.

and 33.41 cycles (N_b), where A stands for aberrant crypts, N is for normal crypts, subscript o is for *β-actin*, a is for *Hexa*, and b is for *Hexb*.

The fluorescence intensity was calculated with the following function, where F is fluorescence intensity, k is constant, X is copy number, and n is cycle number to give the F value for fluorescence (PCR efficiency is considered as 100% here to simplify the calculation, though it was actually reported to be approximately 80%[32)]):

$$F=kX2^n$$

Thus,

$$X=F/(k2^n)$$

So, the corrected copy number (X') normalized with *β-actin* expression level (X_o) is:

$$X'=X/X_o=[F/(k2^n)]/[F/(k_o2^{n_o})]$$

where k_o is a constant and n_o is the cycle number to give the F value for fluorescence for *β-actin*. The formula was simplified as follows (F was arbitrarily set at 9.86 in Fig. 4A):

$$X'=(k_o/k)2^{n_o-n}$$

If a logarithm is taken,

$$\log X'=(n_o-n)\log 2+(\log k_o-\log k)$$

Since $(\log k_o-\log k)$ is a constant, $\log X'$ is proportional to (n_o-n). Therefore, the logarithm of the relative expression level or copy number for *Hexa* and *Hexb* of the aberrant (A) crypts ($\log X'_{Aa}$ and $\log X'_{Ab}$) is proportional to the difference of the crossing points (arrows in the bottom half of Fig. 4A):

$\log X'_{Aa}$ is proportional to $A_o-A_a=25.35-31.02=-5.67$
$\log X'_{Ab}$ is proportional to $A_o-A_b=25.35-34.61=-9.26$

Similarly, for the normal (N) crypt (dotted arrows in the top half of Fig. 4A),

$\log X'_{Na}$ is proportional to $N_o-N_a=29.19-31.43=-2.28$
$\log X'_{Nb}$ is proportional to $N_o-N_b=29.19-33.41=-4.22$

The ratio (R_{Aa}) of *Hexa* in an aberrant crypt compared to that in a normal crypt is:

$$R_{Aa}=X'_{Aa}/X'_{Na}$$

Similarly, the ratio (R_{Ab}) of *Hexb* in an aberrant crypt compared to that in a normal crypt is:

$$R_{Ab}=X'_{Ab}/X'_{Nb}$$

Therefore the logarithm of R_{Aa} and R_{Ab} expression of aberrant compared with normal crypt was calculated as follows (average values in 7 independent experiments and overall average are given in Table II):

$$\log R_{Aa}=\log X'_{Aa}-\log X'_{Na}=-5.67-(-2.28)=-3.39$$
$$\log R_{Ab}=\log X'_{Ab}-\log X'_{Nb}=-9.26-(-4.22)=-5.04$$

where $\log R_{Na}=\log R_{Nb}=0$. Thus, R_{Aa} and R_{Ab} were as follows:

$$R_{Aa}=0.095$$
$$R_{Ab}=0.030$$

where $R_{Na}=R_{Nb}=1$. The same calculation was performed for other aberrant crypts compared with normal ones. Mean−SD, mean, and mean+SD for $\log R_{Aa}$ were −2.72, −1.91, and −1.04 (the right-most column in Table II). Thus, those for R_{Aa} were 0.152, 0.266, and 0.488 (Fig. 4B). Similarly, those for $\log R_{Ab}$ were −4.40, −2.94, and −1.47 (the right-most column in Table II), and or R_{Ab} were 0.047, 0.130, and 0.360 (Fig. 4C).

After the LightCycler reaction, the samples were electrophoresed in 2.5% agarose gels, and visualized with ethidium bromide to confirm that there was no obvious primer dimer formation or amplification of any extra bands. Total RNA samples without reverse transcription (RT) provided no apparent PCR amplification (data not shown).

DISCUSSION

ACF are the earliest preneoplastic lesions found in carcinogen-treated animals and cancer-bearing patients.[33)] For

analysis of ACF at the molecular level, it is necessary to be able to pick out single aberrant crypts in order to exclude adjacent normal crypts and pericryptal fibroblasts and inflammatory cells. Our crypt isolation technique[21, 30] is a powerful method meeting this requirement. However, ACF have so far been defined by their morphologically irregular appearance in methylene blue-stained colonic mucosa. Thus, we have established a simple and reliable method to distinguish aberrant crypts among large numbers of normal ones upon crypt isolation.

To help identify aberrant crypts, functional or biochemical criteria have been utilized. Pretlow *et al.*[9] histochemically revealed ACF to have decreased hexosaminidase activity. EAF have been characterized extensively in the livers of rodents treated with carcinogens.[34–40] Enzyme alterations are also observed in the glandular stomach in carcinogen-treated rodents, so-called pepsinogen-altered pyloric glands (PAPG), also considered as a stomach precancerous lesion.[41–47] We confirmed alteration of hexosaminidase activity by staining of paraformaldehyde-fixed whole mounted colonic mucosa. In contrast to the normal-shaped crypts bearing red grains, ACF remained lightly yellowish. Although, Pretlow *et al.* reported[11] two types of hexosaminidase-decreased lesions including both morphologically altered and apparently normal, there were very few of the latter with decreased hexosaminidase activity in our experiment up to 20 experimental weeks. In our study, hexosaminidase alteration was mostly found in ACF.

The other significant difference between Hex+ and Hex− crypts was in size. The rim diameter of the Hex− crypts was 1.57 times bigger than that of Hex+ ones, and they were therefore 2.46 times larger in terms of surface area. This coincides with the previous report[3] that aberrant crypts occupy 3 to 4 times the space of a normal crypt in mouse colon. The slight discrepancy between these data could be due to species specificity or the difference in measuring methods. Since the width of the crypt showed the largest difference between Hex+ and Hex− crypts, this factor was chosen as a potential marker. The histograms of crypt widths approximated to a normal distribution; the normal range was assumed to be below $\mu_{Hex+}+2\sigma_{Hex+}$ (85.6 μm). Applying the classification proposed by Pretlow *et al.*[11] which included EAF morphologically altered or aberrant (designated as A-EAF, i.e. ACF with decreased hexosaminidase activity) and those that were morphologically normal (N-EAF), Hex− crypts below $\mu_{Hex+}+2\sigma_{Hex+}$ may be N-EAF and ones bigger than that may be A-EAF. Since hexosaminidase staining required samples to be fixed with paraformaldehyde and incubated at 37°C for 1 h, this procedure was not appropriate for isolation of nucleic acids, especially RNA. Therefore, for better preservation, isolated crypts were fixed in 70% ethanol, with which hexosaminidase was inactivated. Thus, for the molecular analysis of ACF, large crypts with twice the average width of Hex+ crypts ($2\times57.6=115.1$ μm) or larger were here selected, allowing 30% of Hex− ACF (large A-EAF) to be recovered with a negligible probability of contaminating Hex+ crypts. Although this selection might have failed to isolate some of the smaller A-EAF and N-EAF having potential for further progression to carcinomas, the population larger than 115 μm in width represented typical ACF with large size and morphological aberration, which have long been thought to be precancerous lesions and have been utilized as a biomarker of colon carcinogenesis.

Individual ACF may have different fates. Some may progress to become malignant tumors. Others may disappear, possibly through an apoptotic mechanism. To predict the outcome, it is necessary to apply molecular biology techniques to analyze the expression levels or mutation status of proliferation- or differentiation-associated genes for each crypt. To confirm that a selected crypt was really a Hex− aberrant crypt, the expression of *Hexa* and *Hexb* was then analyzed. For this purpose, real-time relative quantitative RT-PCR was performed using the LightCycler system.[48–50] Since there were big differences in size between aberrant and normal crypts, it was practically impossible to adjust input amount for an absolute quantitation. Therefore, relative amounts of *Hexa* and *Hexb* mRNAs were quantified with reference to a housekeeping gene, *β-actin*, according to a widely accepted procedure.[32, 51] As shown in Fig. 4A, crossing points (or threshold points) for *β-actin* in normal and aberrant crypts were widely distributed, probably reflecting their size. It would have been difficult to perform quantitation using a conventional PCR method as described by Bird *et al.*[28] Real-time quantitative PCR overcame this difficulty for relative quantitation even for very small samples from colonic crypts.

Hexa and *Hexb* expression levels in aberrant crypts were respectively 27% and 13% of those in normal crypts in rat colon. As *Hexa* and *Hexb* knockout mice[18, 19] have not been reported to have any apparent abnormalities in colonic mucosa, transcriptional down-regulation of these genes seems not to be functionally or structurally important, but seems to be a good molecular marker for dedifferentiation. However, it remains necessary to analyze the knockout mice to confirm the importance of *Hex* gene products during development and progression of ACF through colon cancers.

Here, we described a simple method to distinguish aberrant crypts from normal ones with a previously established crypt isolation technique. Crypts selected on size criteria could be confirmed as functionally or biochemically aberrant by quantification of *Hexa* and *Hexb* mRNA with the LightCycler real-time PCR. Skepticism about whether ACF are all really precancerous lesions for colon cancer

has recently increased. We believe that our technique described here may be utilized to subclassify ACF into those with and without potential for progression, opening new avenues to molecular analysis of individual ACF.

ACKNOWLEDGMENTS

This work was supported in part by Grants-in-Aid for Cancer Research from the Ministry of Health and Welfare, by Grants-in-Aid from the Ministry of Education, Science, Sports and Culture of Japan, by Grants-in-Aid from CREST (Core Research for Evolutional Science and Technology) of the Japan Science and Technology Corporation, by a grant from the Society for Promotion of Pathology of Aichi, Japan, and by the Aichi Cancer Research Foundation. We also thank Ms. Rie Takabayashi for administrative tasks.

(Received June 21, 2000/Revised September 28, 2000/2nd Revised November 10, 2000/Accepted November 18, 2000)

REFERENCES

1) Kinzler, K. W. and Vogelstein, B. Colorectal tumors. *In* "The Genetic Basis of Human Cancer," ed. B. Vogelstein and K. W. Kinzler, pp. 565–587 (1998). McGraw-Hill, New York.
2) Bird, R. P. Observation and quantification of aberrant crypts in the murine colon treated with a colon carcinogen: preliminary findings. *Cancer Lett.*, **37**, 147–151 (1987).
3) McLellan, E. A. and Bird, R. P. Aberrant crypts: potential preneoplastic lesions in the murine colon. *Cancer Res.*, **48**, 6187–6192 (1988).
4) McLellan, E. A., Medline, A. and Bird, R. P. Sequential analyses of the growth and morphological characteristics of aberrant crypt foci: putative preneoplastic lesions. *Cancer Res.*, **51**, 5270–5274 (1991).
5) McLellan, E. A., Medline, A. and Bird, R. P. Dose response and proliferative characteristics of aberrant crypt foci: putative preneoplastic lesions in rat colon. *Carcinogenesis*, **12**, 2093–2098 (1991).
6) Brattain, M. G., Kimball, P. M. and Pretiow, T. G. β-Hexosaminidase isozymes in human colonic carcinoma. *Cancer Res.*, **37**, 731–735 (1977).
7) Brattain, M. G., Green, C., Kimball, P. M., Marks, M. and Khaled, M. Isoenzymes of β-hexosaminidase from normal rat colon and colonic carcinoma. *Cancer Res.*, **39**, 4083–4090 (1979).
8) Freeman, H. J., Kim, Y. and Kim, Y. S. Glycoprotein metabolism in normal proximal and distal rat colon and changes associated with 1,2-dimethylhydrazine-induced colonic neoplasia. *Cancer Res.*, **38**, 3385–3390 (1978).
9) Pretlow, T. P., O'Riordan, M. A., Kolman, M. F. and Jurcisek, J. A. Colonic aberrant crypts in azoxymethane-treated F344 rats have decreased hexosaminidase activity. *Am. J. Pathol.*, **136**, 13–16 (1990).
10) Barrow, B. J., O'Riordan, M. A., Stellato, T. A., Calkins, B. M. and Pretlow, T. P. Enzyme-altered foci in colons of carcinogen-treated rats. *Cancer Res.*, **50**, 1911–1916 (1990).
11) Pretlow, T. P., O'Riordan, M. A., Spancake, K. M. and Pretlow, T. G. Two types of putative preneoplastic lesions identified by hexosaminidase activity in whole-mounts of colons from F344 rats treated with carcinogen. *Am. J. Pathol.*, **142**, 1695–1700 (1993).
12) Pretlow, T. P., Cheyer, C. and O'Riordan, M. A. Aberrant crypt foci and colon tumors in F344 rats have similar increases in proliferative activity. *Int. J. Cancer*, **56**, 599–602 (1994).
13) Pereira, M. A., Barnes, L. H., Rassman, V. L., Kelloff, G. V. and Steele, V. E. Use of azoxymethane-induced foci of aberrant crypts in rat colon to identify potential cancer chemopreventive agents. *Carcinogenesis*, **15**, 1049–1054 (1994).
14) Whiteley, L. O., Hudson, L., Jr. and Pretlow, T. P. Aberrant crypt foci in the colonic mucosa of rats treated with a genotoxic and nongenotoxic colon carcinogen. *Toxicol. Pathol.*, **24**, 681–689 (1996).
15) Tao, L., Li, K. and Pereira, M. A. Chemopreventive agents-induced regression of azoxymethane-induced aberrant crypt foci with the recovery of hexosaminidase activity. *Carcinogenesis*, **18**, 1415–1418 (1997).
16) Sandhoff, K., Conzelmann, E., Neufeld, E. F., Kaback, M. M. and Suzuki, K. The GM2 gangliosidosis. *In* "The Metabolic Basis of Inherited Disease," ed. C. R. Scriver, A. L. Beaudet, W. S. Sly and D. Valle, Vol. 2, pp. 1807–1839 (1989). McGraw-Hill, New York.
17) Yamanaka, S., Johnson, O. N., Norflus, F., Boles, D. J. and Proia, R. L. Structure and expression of the mouse β-hexosaminidase genes, Hexa and Hexb. *Genomics*, **21**, 588–596 (1994).
18) Yamanaka, S., Johnson, M. D., Grinberg, A., Westphal, H., Crawley, J. N., Taniike, M., Suzuki, K. and Proia, R. L. Targeted disruption of the Hexa gene results in mice with biochemical and pathologic features of Tay-Sachs disease. *Proc. Natl. Acad. Sci. USA*, **91**, 9975–9979 (1994).
19) Sango, K., Yamanaka, S., Hoffmann, A., Okuda, Y., Grinberg, A., Westphal, H., McDonald, M. P., Crawley, J. N., Sandhoff, K., Suzuki, K. and Proia, R. L. Mouse models of Tay-Sachs and Sandhoff diseases differ in neurologic phenotype and ganglioside metabolism. *Nat. Genet.*, **11**, 170–176 (1995).
20) Bjerknes, M. and Cheng, H. Methods for the isolation of intact epithelium from the mouse intestine. *Anat. Rec.*, **199**, 565–574 (1981).
21) Fujimitsu, Y., Nakanishi, H., Inada, K., Yamachika, T., Ichinose, M., Fukami, H. and Tatematsu, M. Development of aberrant crypt foci involves a fission mechanism as revealed by isolation of aberrant crypts. *Jpn. J. Cancer Res.*, **87**, 1199–1203 (1996).
22) Tsukamoto, T., Kozaki, K., Nishikawa, Y., Yamamoto, M.,

Fukami, H., Inoue, M., Wakabayashi, K. and Tatematsu, M. Development and distribution of 2-amino-1-methyl-6-phenylimidazo[4,5-*b*]pyridine (PhIP)-induced aberrant crypt foci in the rat large intestine. *Jpn. J. Cancer Res.*, **90**, 720–725 (1999).

23) Hayashi, M. Histochemical demonstration of N-acetyl-β-glucosaminidase employing naphthol AS-BI N-acetyl-β-glucosaminide as substrate. *J. Histochem. Cytochem.*, **13**, 355–360 (1965).
24) Robertson, W. R. A quantitative study of N-acetyl-β-glucosaminidase activity in unfixed tissue sections of the guinea-pig thyroid gland. *Histochem. J.*, **12**, 87–96 (1980).
25) Rosner, B. "Fundamentals of Biostatistics" (1995). Duxbury Press, Wadsworth Publ. Co., Belmont, CA.
26) Chomczynski, P. and Sacchi, N. Single-step method of RNA isolation by acid guanidinium thiocyanate-phenol-chloroform extraction. *Anal. Biochem.*, **162**, 156–159 (1987).
27) Tsukamoto, T., Kusakabe, M. and Saga, Y. *In situ* hybridization with non-radioactive digoxigenin-11-UTP-labeled cRNA probes: localization of developmentally regulated mouse tenascin mRNAs. *Int. J. Dev. Biol.*, **35**, 25–32 (1991).
28) Bird, R. P., Salo, D., Lasko, C. and Good, C. A novel methodological approach to study the level of specific protein and gene expression in aberrant crypt foci putative preneoplastic colonic lesions by Western blotting and RT-PCR. *Cancer Lett.*, **116**, 15–19 (1997).
29) Tsukamoto, T., Takahashi, T., Ueda, R., Hibi, K., Saito, H. and Takahashi, T. Molecular analysis of the protein tyrosine phosphatase gamma gene in human lung cancer cell lines. *Cancer Res.*, **52**, 3506–3509 (1992).
30) Tsukamoto, T., Huang, T., Guzman, R. C., Chen, X., Pascual, R. V., Kitamura, T. and Nandi, S. Isolation of oncogenes from rat mammary tumors by a highly efficient retrovirus expression cloning system. *Biochem. Biophys. Res. Commun.*, **265**, 7–12 (1999).
31) Nudel, U., Zakut, R., Shani, M., Neuman, S., Levy, Z. and Yaffe, D. The nucleotide sequence of the rat cytoplasmic β-actin gene. *Nucleic Acids Res.*, **11**, 1759–1771 (1983).
32) Freeman, W. M., Walker, S. J. and Vrana, K. E. Quantitative RT-PCR: pitfalls and potential. *Biotechniques*, **26**, 112–125 (1999).
33) Bird, R. P. Role of aberrant crypt foci in understanding the pathogenesis of colon cancer. *Cancer Lett.*, **93**, 55–71 (1995).
34) Mellors, R. C. and Sugiura, K. Alkaline phosphatase activity and basophilia in hepatic cells following administration of butter yellow to rats. *Proc. Soc. Exp. Biol. Med.*, **67**, 242–246 (1948).
35) Kalengayi, M. M., Ronchi, G. and Desmet, V. J. Histochemistry of gamma-glutamyl transpeptidase in rat liver during aflatoxin B1-induced carcinogenesis. *J. Natl. Cancer Inst.*, **55**, 579–588 (1975).
36) Shinozuka, H., Sells, M. A., Katyal, S. L., Sell, S. and Lombardi, B. Effects of a choline-devoid diet on the emergence of gamma-glutamyltranspeptidase-positive foci in the liver of carcinogen-treated rats. *Cancer Res.*, **39**, 2515–2521 (1979).
37) Peraino, C., Richards, W. L. and Stevens, F. J. Multistage hepatocarcinogenesis. *In* "Mechanisms of Tumor Promotion," ed. T. J. Slaga, Vol. 1, pp. 1–58 (1983). CRC Press, Boca Raton, FL.
38) Hei, T. K. and Sudilovsky, O. Effects of a high-sucrose diet on the development of enzyme-altered foci in chemical hepatocarcinogenesis in rats. *Cancer Res.*, **45**, 2700–2705 (1985).
39) Boberg, E. W., Liem, A., Miller, E. C. and Miller, J. A. Inhibition by pentachlorophenol of the initiating and promoting activities of 1′-hydroxysafrole for the formation of enzyme-altered foci and tumors in rat liver. *Carcinogenesis*, **8**, 531–539 (1987).
40) Pretlow, T. P., Grane, R. W., Goehring, P. L., Lapinsky, A. S. and Pretlow, T. G. Examination of enzyme-altered foci with gamma-glutamyl transpeptidase, aldehyde dehydrogenase, glucose-6-phosphate dehydrogenase, and other markers in methacrylate-embedded liver. *Lab. Invest.*, **56**, 96–100 (1987).
41) Tatematsu, M., Furihata, C., Mera, Y., Shirai, T., Matsushima, T. and Ito, N. Immunohistochemical demonstration of induction of pyloric glands with low pepsinogen 1 (Pg 1) content in rat stomach by N-methyl-N′-nitro-N-nitrosoguanidine. *Jpn. J. Cancer Res.* (Gann), **77**, 238–243 (1986).
42) Tatematsu, M., Furihata, C., Katsuyama, T., Mera, Y., Inoue, T., Matsushima, T. and Ito, N. Immunohistochemical demonstration of pyloric gland-type cells with low-pepsinogen isozyme 1 in preneoplastic and neoplastic tissues of rat stomachs treated with N-methyl-N′-nitro-N-nitrosoguanidine. *J. Natl. Cancer Inst.*, **78**, 771–777 (1987).
43) Tatematsu, M., Mutai, M., Inoue, K., Ozaki, K., Furihata, C. and Ito, N. Synergism between sodium chloride and sodium taurocholate and development of pepsinogen-altered pyloric glands: relevance to a medium-term bioassay system for gastric carcinogens and promoters in rats. *Jpn. J. Cancer Res.*, **80**, 1035–1040 (1989).
44) Tatematsu, M., Mutai, M., Aoki, T., de Camargo, J. L., Furihata, C. and Ito, N. Proliferation kinetics of pepsinogen altered pyloric gland cells in rats treated with N-methyl-N′-nitro-N-nitrosoguanidine. *Carcinogenesis*, **10**, 907–911 (1989).
45) Tatematsu, M., Ozaki, K., Mutai, M., Shichino, Y., Furihata, C. and Ito, N. Enhancing effects of various gastric carcinogens on development of pepsinogen-altered pyloric glands in rats. *Carcinogenesis*, **11**, 1975–1978 (1990).
46) Tatematsu, M., Ichinose, M., Tsukada, S., Kakei, N., Takahashi, S., Ogawa, K., Hirose, M., Furihata, C., Miki, K., Kurokawa, K. and Ito, N. DNA methylation of the pepsinogen 1 gene during rat glandular stomach carcinogenesis induced by N-methyl-N′-nitro-N-nitrosoguanidine or cate-

chol. *Carcinogenesis*, **14**, 1415–1419 (1993).
47) Yamamoto, M., Furihata, C., Fujimitsu, Y., Imai, T., Inada, K., Nakanishi, H. and Tatematsu, M. Dose-dependent induction of both pepsinogen-altered pyloric glands and adenocarcinomas in the glandular stomach of C3H mice treated with *N*-methyl-*N*-nitrosourea. *Jpn. J. Cancer Res.*, **88**, 238–244 (1997).
48) Wittwer, C. T., Ririe, K. M., Andrew, R. V., David, D. A., Gundry, R. A. and Balis, U. J. The LightCycler: a microvolume multisample fluorimeter with rapid temperature control. *Biotechniques*, **22**, 176–181 (1997).
49) Wittwer, C. T., Herrmann, M. G., Moss, A. A. and Rasmussen, R. P. Continuous fluorescence monitoring of rapid cycle DNA amplification. *Biotechniques*, **22**, 130–138 (1997).
50) Morrison, T. B., Weis, J. J. and Wittwer, C. T. Quantification of low-copy transcripts by continuous SYBR Green I monitoring during amplification. *Biotechniques*, **24**, 954–958, 960, 962 (1998).
51) Heid, C. A., Stevens, J., Livak, K. J. and Williams, P. M. Real time quantitative PCR. *Genome Res.*, **6**, 986–994 (1996).